2015

Monolithic optofluidic ring resonator lasers created by femtosecond laser nanofabrication

Hengky Chandrahalim
Air Force Institute of Technology

Qiushu Chen

Ali A. Said

Mark Dugan

Xudong Fan

Recommended Citation

Hengky Chandrahalim, Qiushu Chen, Ali A. Said, Mark Dugan, and Xudong Fan, "Monolithic optofluidic ring resonator lasers created by femtosecond laser nanofabrication," Lab Chip, 15, 2015, pp. 2335-2340. https://doi.org/10.1039/c5lc00254k

Lab on a Chip

PAPER

Monolithic optofluidic ring resonator lasers created by femtosecond laser nanofabrication†

Cite this: DOI: 10.1039/c5lc00254k

Hengky Chandrahalim,[a] Qiushu Chen,[a] Ali A. Said,[b] Mark Dugan[b] and Xudong Fan*[a]

Received 4th March 2015,
Accepted 9th April 2015

DOI: 10.1039/c5lc00254k

www.rsc.org/loc

We designed, fabricated, and characterized a monolithically integrated optofluidic ring resonator laser that is mechanically, thermally, and chemically robust. The entire device, including the ring resonator channel and sample delivery microfluidics, was created in a block of fused-silica glass using a 3-dimensional femtosecond laser writing process. The gain medium, composed of Rhodamine 6G (R6G) dissolved in quinoline, was flowed through the ring resonator. Lasing was achieved at a pump threshold of approximately 15 μJ mm^{-2}. Detailed analysis shows that the Q-factor of the optofluidic ring resonator is 3.3×10^4, which is limited by both solvent absorption and scattering loss. In particular, a Q-factor resulting from the scattering loss can be as high as 4.2×10^4, suggesting the feasibility of using a femtosecond laser to create high quality optical cavities.

Introduction

The fusion of optics and fluidics has given birth to the flourishing field of optofluidics, in which optical elements and fluidic frameworks are amalgamated on a common substrate to synergistically deliver a broad range of functionalities and high performances.[1–3] Optofluidic lasers are among the branches of optofluidics that promise solutions to the presently insurmountable problems.[1,4,5] They have justified themselves to be outstanding nominees for on-chip tunable coherent light sources,[6–8] bio-controlled lasers,[9] and sensitively analyzing biomolecules.[5,10–14] The earlier debuts of optofluidic lasers[15–18] with notable features have sparked a resurgence of research interest in exploring various optical cavity architectures, device materials, fluidic gain media, and fabrication technologies to promote broader applications.

From a manufacturing point of view, a successful deployment of optofluidic lasers as practical sub-modules in lab-on-a-chip (LOC) design requires a simple process that can reliably produce the desirable apparatuses while providing a great degree of design freedom. The ideal fabrication process should be compatible with rapid prototyping and relatively low cost. From a device application standpoint, a platform that has high mechanical strength, broad chemical compatibility, and good thermal stability is highly favorable.

In the last decade, several research groups have demonstrated Bragg gratings based optofluidic lasers, such as distributed feedback (DFB) laser on a chip.[8,19–22] These devices exhibit certain compelling characteristics, such as low pump thresholds, tunable wavelengths, and single mode of operations. However, the manufacturing of these devices is not straightforward and rather expensive as electron-beam (e-beam) lithography is used for patterning the gratings in conjunction with additional multilayer processing steps. Microfluidic dye lasers that integrate a Fabry–Pérot cavity with two fiber-based mirrors have shown single mode emissions and digital programmability.[6,17,23,24] Nevertheless, the coating process of the Fabry–Pérot cavity is an arduous process, which is difficult to implement in a monolithically integrated system. Furthermore, this type of optofluidic laser entails a multipart assembly process, which degrades the compactness and robustness of the device. Fabry–Pérot microcavity fluidic dye lasers with metallic mirrors have also been reported previously.[16,25] While these devices can be expediently integrated with other microfluidic systems without adding further processing steps, the overall fabrication and assembly processes either are relatively long and complicated,[16] or have to be accomplished manually by adding spacer beads.[25] Furthermore, the polymer bonding process may raise issues associated with imprecisions and device sturdiness. More recently, an optofluidic laser based on a two-dimensional photonic crystal[26] was demonstrated. This device was patterned by a laser interference lithography[27] technique. It reveals enhanced spontaneous emissions and a low laser threshold of 9×10^3 nJ cm^{-2}. Although the laser interference lithography seems to have evaded the necessity of employing expensive and tedious e-beam lithography process, it demands very customized

[a] Department of Biomedical Engineering, University of Michigan, Ann Arbor, MI 48109, USA. E-mail: xsfan@umich.edu
[b] Translume Inc., 655 Phoenix Drive, Ann Arbor, MI, USA

† Electronic supplementary information (ESI) available. See DOI: 10.1039/c5lc00254k

and laborious optical alignments to pattern each device with particular dimensions. This patterning method may be suitable to accurately realize a large array of devices with high resolutions and optical sub-wavelength dimensions for various laboratory experiments, but it is very challenging to adopt this process to manufacture and integrate practical devices as this type of lithography technique is incapable of patterning arbitrary shapes.

The ring-shaped optical cavities that operate based on the whispering gallery modes (WGM) are known to have relatively high quality factors (Q-factors) even when they are fabricated on a chip.[28–30] They have a simple form factor, miniscule size, ability to support a broad range of lasing emission wavelengths, and do not demand space consuming arrays of identical nanoscale structures which require e-beam patterning such as Bragg grating based devices. Optofluidic ring resonator dye lasers that have compact sizes and single mode of operations have been previously presented.[31–33] However, they were built on materials (such as polydimethylsiloxane) with very modest flexural rigidity and limited chemical compatibility, making it challenging to operate these devices under practical conditions. More importantly, the *planar* lithography method that is used to pattern those devices makes it extremely difficult to deliver liquid gain medium into the ring resonator without degrading its optical performance, including its Q-factor.

The present work focuses on the design, fabrication, and characterization of a monolithically integrated optofluidic ring resonator laser that meets the requirements put forth earlier. We fabricated the entire device, including the ring resonator and the microfluidics, with a relatively simple femtosecond laser direct-writing, followed by a wet chemical etching, and a final thermal bonding. This integration concept is appealing for many lab-on-a-chip applications: it has manifold advantages, such as reproducible fabrication, straightforward assembly, and does not require post-fabrication processes such as dicing and packaging. These are all originated from the fact that we are engaged to a single piece of material.[34] In addition, the 3-D fluidic design enabled by the femtosecond laser fabrication allows to deliver the liquid gain medium to the ring resonator without affecting significantly its optical performance or degrading the cavity Q-factor as discussed later. Note that previously Cheng *et al.* demonstrated dye lasers with four micro-mirrors machined using a femtosecond laser.[15] Nonetheless, the cavity occupied a relatively large area and has a low Q-factor due to the stringent requirements for the micro-mirror's surfaces imposed by the device configuration.

Our optofluidic ring resonator laser was characterized using Rhodamine 6G (R6G) dye dissolved in a quinoline solution (n = 1.62) as the gain medium and optically pumped by nanosecond pulses generated by a 532 nm optical parametric oscillator (OPO). The laser emission emerged at 575 nm wavelength with a relatively low pump threshold fluence of ~15 μJ mm^{-2} per pulse. We observed stable laser emissions for different dye concentrations. Furthermore, by analyzing the lasing threshold, a bare cavity Q-factor of 3.3 × 10^4 is deduced. Lasing with R6G in chlorobenzene (n = 1.524) was also demonstrated.

Design and fabrication

The optofluidic ring resonator laser in this work predominantly comprised of a ring-shaped channel to define the liquid cavity and connecting microfluidic channels used to flow the gain medium solution. All components that build the laser were monolithically incorporated in a piece of fused-silica glass with 3-D freedom. The top and cross-sectional views of the device are illustrated in Fig. 1. The ring cavity was designed to have inner and outer radii and depth of 150 μm, 170 μm, and 40 μm, respectively.

Owing to the capability of the femtosecond laser to tailor the microfluidic channels in three dimensions, we are able to introduce fluidic channels to transport the gain medium from the *inner* circumference of the ring where virtually no WGM is present (Fig. 1(A)). This design concept, in contrast to the ring cavity in ref. 32 where the liquid waveguide channel has to merge with the liquid ring resonator channel for sample delivery, eliminates the possible source of Q-factor degradation.[35] In addition, the vertical fluidic channels with direct contact to the ring are built to have smaller cross-sectional dimensions (10 μm × 20 μm) than the ring to serve

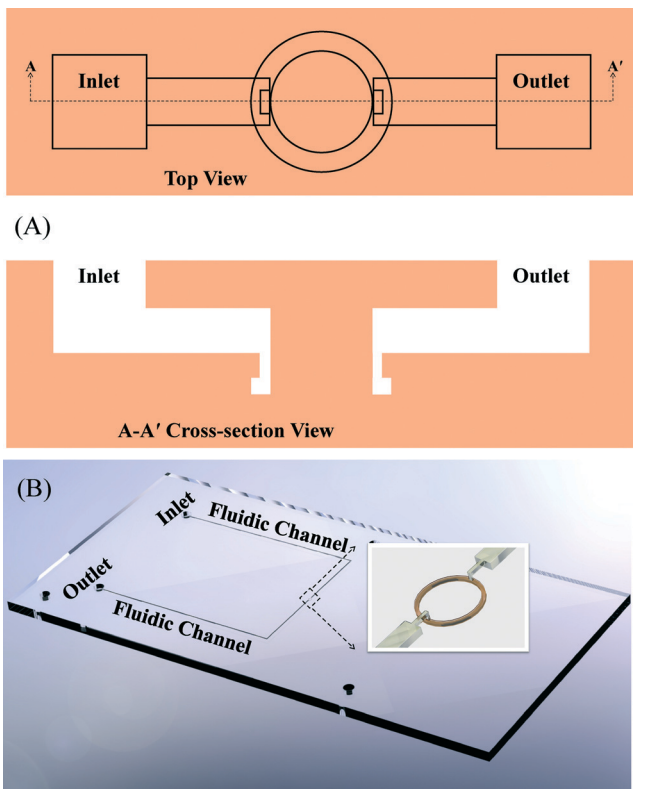

Fig. 1 (A) Top and cross-sectional view of the monolithic optofluidic ring resonator. (B) CAD design of the optofluidic system. Inset shows the details of the ring resonator and the fluidics that delivers the gain solution into the ring resonator.

as high flow resistances that guarantee the cavity is constantly filled with adequate amount of light amplification medium irrespective to the device orientation (see the inset in Fig. 1(B)).

The machining process was started with two fused silica substrates with identical dimensions of 1 inch × 2 inch. The optofluidic components were initially machined separately in these two substrates, with one piece containing the microring and the other encompassing the remaining microfluidic elements, including the input and output fluidic ports. The fabrication process is comprised of three main steps: in the first step, the external boundaries of the various microfluidic elements are written in their respective substrates. This writing step consists of exposing the substrates to femtosecond laser pulses from a Ti:sapphire laser operating at 800 nm. The pulse width is approximately 100 fs and the repetition rate is set at 250 kHz. The beam is focused into the sample with a long-working distance microscope objective. The laser writing speed ranges from 100 μm s^{-1} to 5 mm s^{-1} depending on the local geometry of the optofluidic element. The laser pulse energy is adjusted so that there is no material ablation associated with this first step. Both transverse and longitudinal polarizations of the laser beam are used for the exposure. After the laser exposure is completed, the fused-silica substrates are immersed in a low-concentration aqueous solution of hydrofluoric acid. The specimens are polished and rinsed multiple times. Finally, the two substrates are aligned in a clean room and fused together in a high-temperature furnace to form a monolithic optofluidic system. The photograph of the laser-machined device and the microphotograph of the microring cavity are shown in Fig. 2. Fig. 2(B) and (C) present the images of the microring and adjoining fluidic channels taken at different focal lengths. The optical measurements suggest that the separation distance between the ring and parallel fluidic channels is approximately 100 μm, which is in agreement with the design specification. Fig. 2(C) also evidently points out that the orthogonal fluidic channels which directly contact the ring are routed from the inner circumference of the ring.

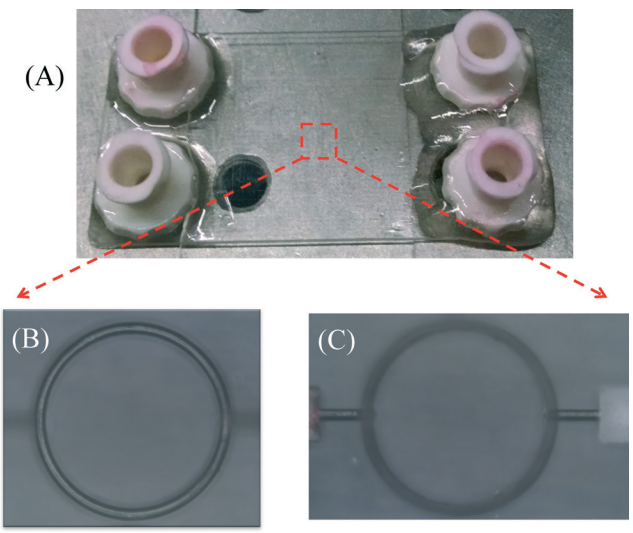

Fig. 2 (A) Picture of the optofluidic ring resonator laser system. (B) and (C) Microscopic pictures of the optofluidic ring resonator focused on the ring and the fluid delivery channel, respectively.

Experimental

The optofluidic laser was tested according to the measurement setup outlined in Fig. 3. Chemically inert polytetrafluoroethylene (PTFE) tubes with an inner diameter of 300 μm were attached to the input and output fluidic ports as shown in Fig. 3(B). The RG6 dye was dissolved in quinoline: the concentration was 1 mM. The gain solution was then injected into the fluidic channel at a constant flow rate of 3 μL min^{-1} using a syringe pump. The aqueous cavity was formed as the active solution with a higher refractive index (1.62) than that of the circumambient fused-silica (1.46) inhabits the ring channel. Next, nanosecond pulses at 532 nm wavelength with 20 Hz repetition rate were launched from an optical parametric oscillator to excite the cavity. The pump beam was focused to a spot area of 0.33 mm^2 on the sample by using a cylindrical lens. The coherent light output was emitted from the optofluidic cavity and recorded by a

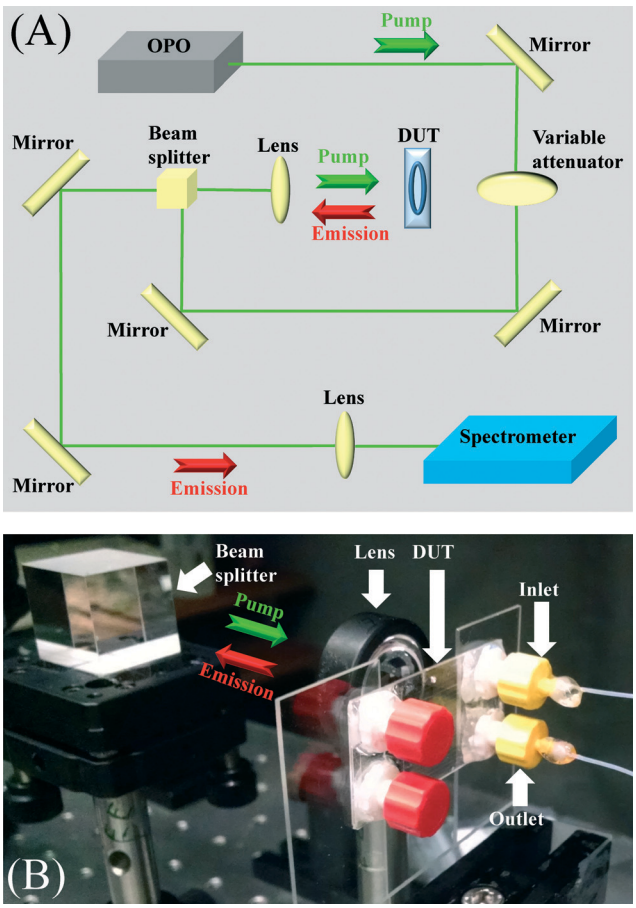

Fig. 3 (A) Schematic of the measurement setup. (B) A close-up view of the device under test during measurement.

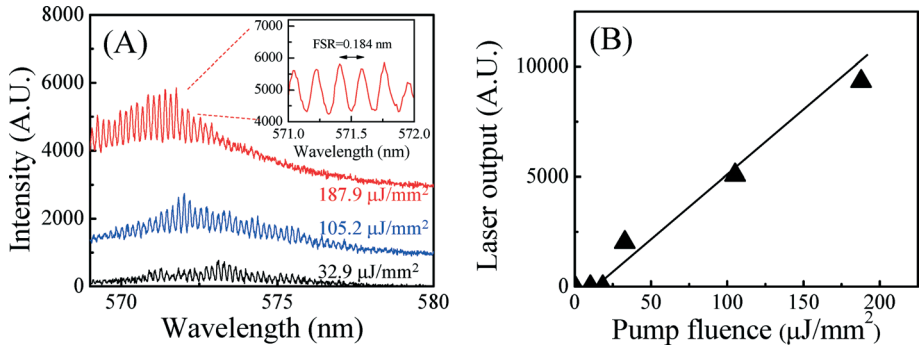

Fig. 4 (A) Lasing spectrum of the optofluidic ring resonator dye laser with a pump fluence of 187.9 μJ mm^{-2} per pulse, 1 mM of R6G dye in quinoline, and a flow rate of 3 μL min^{-1}. The spot size of the OPO pumping laser beam was approximately 0.33 mm^2. A 2400 g mm^{-1} grating was used to achieve high spectral resolution (~0.05 nm). Broad fluorescence background is removed. Spectra are vertically shifted for clarity. Inset: a magnified portion around 572 nm, showing a free spectral range of 0.184 nm. Wider spectral coverage lasing spectra below and just above the threshold are given in Fig. S1.† (B) Spectrally integrated (569–576 nm) laser output as a function of pump fluence extracted from (A). The lasing threshold is approximately 15 μJ mm^{-2}. Solid line is the linear fit above the threshold.

spectrometer (Horiba iHR550, 2400 g mm^{-1} grating, spectral resolution: ~0.05 nm, unless otherwise noted) (Fig. 3(A)).

Results and discussion

Fig. S1† plots the evolution of the emission from the ring resonator when the pump intensity increases. At low pump intensity, only broad fluorescence centered around 567 nm appears. With further increase in pump, multiple laser emission peaks emerge at the red-side of the fluorescence spectrum. Fig. 4(A) shows the high resolution lasing spectra, which allows us to distinguish each lasing peak. The free-spectral-range (FSR) of approximately 0.184 nm is clearly seen near the wavelength of 572 nm. This FSR is very close to the theoretical prediction of 0.189 nm using FSR = $\lambda_m^2/(2\pi r n_{Eff})$, where λ_m = 572 nm, r = 170 μm, n_{Eff} = 1.62, which suggests that the laser mode travels along the outer rim of the ring resonator, as expected. At pump intensity well above the threshold, a small blue shift in the lasing peak is observed, consistent with what was previously reported.[36] Fig. 4(B) displays the spectrally integrated laser emission as a function of the pump intensity. The lasing threshold is approximated 15 μJ mm^{-2}. To further confirm the laser emission, additional experiments were performed with lower concentrations of RG6 dye in quinoline. Blue shifts in the laser emissions accompanied by attenuations in output peak intensity were recorded as the concentration of RG6 was lowered from 1 to 0.5 and 0.38 mM while preserving the same pump intensity as shown in Fig. 5(A)–(C). The dependence of emission wavelengths on the dye concentrations has been previously studied[36,37] and can be accounted for by the dye laser theory presented in the ESI.† The versatility of the optofluidic ring resonator laser lies in its capability to conveniently change the solvent (and gain medium as well). Fig. S8† shows that the lasing emission can easily be achieved with R6G dissolved in chlorobenzene (n = 1.524).

Success of ring resonator fabrication by femtosecond laser writing technology is reflected in the resonator's bare cavity Q-factor, Q_0 (*i.e.*, the Q-factor in the absence of the gain medium). The Q-factor in the previous work, although not reported, is expected to be rather low due to the low reflectivity of the mirrors.[15] In the current work, it is difficult to directly measure Q_0. However, as detailed in the ESI,† the lasing threshold analysis is able to provide quite accurate Q_0 estimation. Based on the lasing fluence threshold of 15 μJ mm^{-2}, we estimate $Q_0 = 3.3 \times 10^4$.

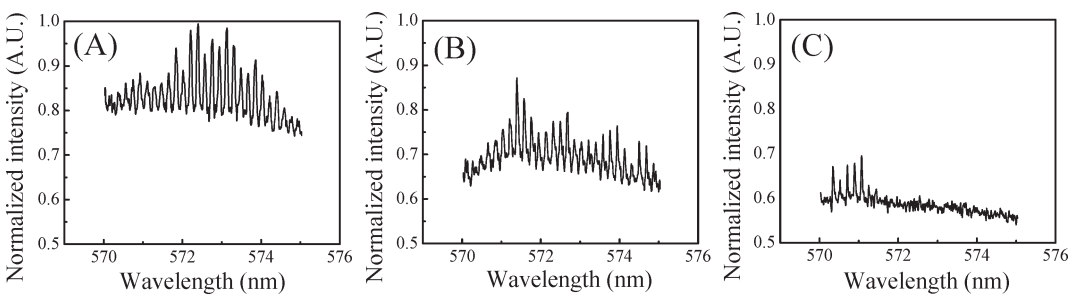

Fig. 5 Blue shifts in the laser emissions accompanied by reduction in output peak intensity as the concentration of RG6 dye was decreased from 1 mM (A) to 0.5 mM (B) and finally to 0.38 mM (C) while keeping the same pump fluence (105.2 μJ mm^{-2}). All spectra are normalized with respect to the highest intensity peak recorded in Fig. 5(A).

It is well known that Q_0 is primarily determined by:

$$\frac{1}{Q_0} = \frac{1}{Q_{\mathrm{Rad}}} + \frac{1}{Q_{\mathrm{Sol}}} + \frac{1}{Q_{\mathrm{Sc}}}, \quad (1)$$

where Q_{Rad}, Q_{Sol}, and Q_{Sc} are the Q-factors due to the radiative loss, solvent absorption, and loss resulting from wall scattering. Among the three contributing Q-factors, the loss due to radiation is known to be very small ($Q_{\mathrm{Rad}} > 10^{11}$)[38] due to the relatively large ring radius (170 μm) and high refractive index contrast (Δn ~ 0.17). $Q_{\mathrm{Sol}} = 2\pi n_{\mathrm{Sol}}/\lambda_{\mathrm{L}}\alpha_{\mathrm{Sol}}$, where λ_{L} and α_{Sol} are respectively the lasing wavelength and the absorption coefficient of the solvent. For quinoline, α_{Sol} = 1.1 cm^{-1} (see Fig. S6†), which results in $Q_{\mathrm{Sol}} = 1.6 \times 10^5$. Thus, we can conclude that $Q_{\mathrm{Sc}} = 4.2 \times 10^4$ and Q_0 is mainly determined by the losses due to light scattering from the fused-silica walls and absorption in quinoline. Note that although Q_0 (or Q_{Sc}) is 20–30 times lower than the best previously reported femtosecond laser fabricated ring resonator (Q = 10^6),[39] which underwent CO_2 laser annealing, it still represents one of the best cavities in optofluidic lasers (for example, the Q-factor for DFB and Fabry–Pérot are usually on the order of 10^3 or lower). Such achievement suggests the feasibility of using a femtosecond laser to create high quality optical cavities.

Conclusions and future work

An integrated optofluidic ring resonator laser in a fused-silica glass substrate has been successfully designed, fabricated, and characterized. The manufacturing procedure of this optofluidic laser is unique and compelling for various applications as it offers maskless and flexible fabrication process, easy assembly, excellent device robustness, no post-fabrication processes, quick prototyping, and relatively low cost. The bare cavity Q-factor of 3.3×10^4 has been achieved, suggesting that the femtosecond writing technology can be used to create high quality cavities.

Several characteristics of this proof-of-concept device are entitled for further investigations. First, we will incorporate another liquid ring resonator nearby to achieve single mode of laser operation *via* the Vernier effect.[31,32] In addition, since each ring resonator can be independently controlled, a wavelength-tunable laser will be built by changing the solution in one of the rings. A waveguide can also be fabricated in the vicinity of the ring so that the laser emission can be directionally coupled out. Furthermore, we will explore other high index and low absorption solvents[40] as alternatives to quinoline (see example in Fig. S8†). With those solvents, we expect Q_0 to approach Q_{Sc}, which is caused during femtosecond laser fabrication. Post-fabrication annealing will also be employed to further reduce scattering and increase Q_{Sc}. Finally, biolasers will be explored where gain media such as nanoparticles, biological molecules, and cells will be flowed through the ring resonator.[5]

Acknowledgements

The authors thank the National Institutes of Health (NIBIB-1R21EB016783) and National Science Foundation (ECCS-1303499) for financial supports, Seung Yup Lee and Dr. Mary-Ann Mycek for assistance with the fluorescence lifetime measurement, Zhizheng Zhang for assistance in acquiring SEM images, and Dr. Alper Kiraz and Dr. Aghapi Mordovanakis for valuable discussions.

References

1 X. Fan and I. M. White, Optofluidic microsystems for chemical and biological analysis, *Nat. Photonics*, 2011, **5**, 591–597.
2 D. Psaltis, S. R. Quake and C. Yang, Developing optofluidic technology through the fusion of microfluidics and optics, *Nature*, 2006, **442**, 381–386.
3 H. Schmidt and A. R. Hawkins, The photonic integration of non-solid media using optofluidics, *Nat. Photonics*, 2011, **5**, 598–604.
4 Z. Li and D. Psaltis, Optofluidic dye lasers, *Microfluid. Nanofluid.*, 2007, **4**, 145–158.
5 X. Fan and S.-H. Yun, The potential of optofluidic biolasers, *Nat. Methods*, 2014, **11**, 141–147.
6 G. Aubry, S. Méance, A.-M. Haghiri-Gosnet and Q. Kou, Flow rate based control of wavelength emission in a multicolor microfluidic dye laser, *Microelectron. Eng.*, 2010, **87**, 765–768.
7 M. Gersborg-Hansen and A. Kristensen, Tunability of optofluidic distributed feedback dye lasers, *Opt. Express*, 2007, **15**, 137–142.
8 Z. Li, Z. Zhang, A. Scherer and D. Psaltis, Mechanically tunable optofluidic distributed feedback dye laser, *Opt. Express*, 2006, **14**, 10494–10499.
9 Y. Sun, S. I. Shopova, C.-S. Wu, S. Arnold and X. Fan, Bioinspired optofluidic FRET lasers *via* DNA scaffolds, *Proc. Natl. Acad. Sci. U. S. A.*, 2010, **107**, 16039–16042.
10 Q. Chen, M. Ritt, S. Sivaramakrishnan, Y. Sun and X. Fan, Optofluidic lasers with a single molecular layer of gain, *Lab Chip*, 2014, **14**, 4590–4595.
11 Q. Chen, X. Zhang, Y. Sun, M. Ritt, S. Sivaramakrishnan and X. Fan, Highly sensitive fluorescent protein FRET detection using optofluidic lasers, *Lab Chip*, 2013, **13**, 2679–2681.
12 M. C. Gather and S. H. Yun, Single-cell biological lasers, *Nat. Photonics*, 2011, **5**, 406–410.
13 Y. Sun and X. Fan, Distinguishing DNA by analog-to-digital-like conversion by using optofluidic lasers, *Angew. Chem., Int. Ed.*, 2012, **51**, 1236–1239.
14 X. Zhang, W. Lee and X. Fan, Bio-switchable optofluidic lasers based on DNA Holliday junctions, *Lab Chip*, 2012, **12**, 3673–3675.
15 Y. Cheng, K. Sugioka and K. Midorikawa, Microfluidic laser embedded in glass by three-dimensional femtosecond laser microprocessing, *Opt. Lett.*, 2004, **29**, 2007–2009.
16 B. Helbo, A. Kristensen and A. Menon, A micro-cavity fluidic dye laser, *J. Micromech. Microeng.*, 2003, **13**, 307.

17 Q. Kou, I. Yesilyurt, G. Escalier, J. C. Galas, L. Coureau and Y. Chen, Microfluidic dye laser integration in a lab-on-a-chip device, in *Photonics Asia 2004*, International Society for Optics and Photonics, 2004, pp. 112–115.

18 S. I. Shopova, H. Zhu, X. Fan and P. Zhang, Optofluidic ring resonator based dye laser, *Appl. Phys. Lett.*, 2007, **90**, 221101.

19 Y. Chen, Z. Li, Z. Zhang, D. Psaltis and A. Scherer, Nanoimprinted circular grating distributed feedback dye laser, *Appl. Phys. Lett.*, 2007, **91**, 051109.

20 W. Song, A. E. Vasdekis, Z. Li and D. Psaltis, Optofluidic evanescent dye laser based on a distributed feedback circular grating, *Appl. Phys. Lett.*, 2009, **94**, 161110.

21 C. Vannahme, C. L. Smith, M. B. Christiansen and A. Kristensen, Emission wavelength of multilayer distributed feedback dye lasers, *Appl. Phys. Lett.*, 2012, **101**, 151123.

22 T. Wienhold, F. Breithaupt, C. Vannahme, M. B. Christiansen, W. Dörfler, A. Kristensen and T. Mappes, Diffusion driven optofluidic dye lasers encapsulated into polymer chips, *Lab Chip*, 2012, **12**, 3734–3739.

23 G. Aubry, Q. Kou, J. Soto-Velasco, C. Wang, S. Meance, J. He and A. Haghiri-Gosnet, A multicolor microfluidic droplet dye laser with single mode emission, *Appl. Phys. Lett.*, 2011, **98**, 111111.

24 Q. Kou, I. Yesilyurt and Y. Chen, Collinear dual-color laser emission from a microfluidic dye laser, *Appl. Phys. Lett.*, 2006, **88**, 091101.

25 A. J. C. Kuehne, M. C. Gather, I. A. Eydelnant, S.-H. Yun, D. A. Weitzad and A. R. Wheeler, A switchable digital microfluidic droplet dye-laser, *Lab Chip*, 2011, **11**, 3716–3719.

26 B. Zhen, S.-L. Chua, J. Lee, A. W. Rodriguez, X. Liang, S. G. Johnson, J. D. Joannopoulos, M. Soljačić and O. Shapira, Enabling enhanced emission and low-threshold lasing of organic molecules using special Fano resonances of macroscopic photonic crystals, *Proc. Natl. Acad. Sci. U. S. A.*, 2013, **110**, 13711–13716.

27 J. Lee, B. Zhen, S.-L. Chua, W. Qiu, J. D. Joannopoulos, M. Soljačić and O. Shapira, Observation and differentiation of unique high-*Q* optical resonances near zero wave vector in macroscopic photonic crystal slabs, *Phys. Rev. Lett.*, 2012, **109**, 067401.

28 P. De Heyn, D. Vermeulen, D. Van Thourhout and G. Roelkens, Silicon-on-insulator all-pass microring resonators using a polarization rotating coupling section, *IEEE Photonics Technol. Lett.*, 2012, **24**, 1176–1178.

29 A. Griffith, J. Cardenas, C. B. Poitras and M. Lipson, High quality factor and high confinement silicon resonators using etchless process, *Opt. Express*, 2012, **20**, 21341–21345.

30 B. Momeni, S. Yegnanarayanan, M. Soltani, A. A. Eftekhar, E. S. Hosseini and A. Adibi, Silicon nanophotonic devices for integrated sensing, *J. Nanophotonics*, 2009, **3**, 031001.

31 W. Lee, H. Li, J. D. Suter, K. Reddy, Y. Sun and X. Fan, Tunable single mode lasing from an on-chip optofluidic ring resonator laser, *Appl. Phys. Lett.*, 2011, **98**, 061103.

32 Z. Li, Optofluidic coupled micro-ring resonators for biosensing, in *Frequency Control Symposium (FCS)*, 2012 IEEE International, IEEE, 2012, pp. 1–4.

33 S. K. Tang, Z. Li, A. R. Abate, J. J. Agresti, D. A. Weitz, D. Psaltis and G. M. Whitesides, A multi-color fast-switching microfluidic droplet dye laser, *Lab Chip*, 2009, **9**, 2767–2771.

34 Y. Bellouard, A. A. Said, M. Dugan and P. Bado, All-optical, ultra-high accuracy displacement sensors with detection means, in *European Symposium on Optics and Photonics for Defence and Security*, International Society for Optics and Photonics, Belgium, 2005, p. 59890V-59891-59814.

35 B. E. Little, J. Foresi, G. Steinmeyer, E. Thoen, S. Chu, H. Haus, E. Ippen, L. Kimerling and W. Greene, Ultra-compact $Si–SiO_2$ microring resonator optical channel dropping filters, *IEEE Photonics Technol. Lett.*, 1998, **10**, 549–551.

36 S. Lacey, I. M. White, Y. Sun, S. I. Shopova, J. M. Cupps, P. Zhang and X. Fan, Versatile opto-fluidic ring resonator lasers with ultra-low threshold, *Opt. Express*, 2007, **15**, 15523–15530.

37 D. V. Vezenov, B. T. Mayers, D. B. Wolfe and G. M. Whitesides, Integrated fluorescent light source for optofluidic applications, *Appl. Phys. Lett.*, 2005, **86**, 041104.

38 M. L. Gorodetsky, A. A. Savchenkov and V. S. Ilchenko, Ultimate *Q* of optical microsphere resonators, *Opt. Lett.*, 1996, **21**, 453–455.

39 J. Lin, S. Yu, Y. Ma, W. Fang, F. He, L. Qiao, L. Tong, Y. Cheng and Z. Xu, On-chip three-dimensional high-*Q* microcavities fabricated by femtosecond laser direct writing, *Opt. Express*, 2012, **20**, 10212–10217.

40 J. Stone, Measurements of the absorption of light in low-loss liquids, *J. Opt. Soc. Am.*, 1972, **62**, 327–333.

Electronic Supplementary Material (ESI) for Lab on a Chip.

Supplementary Information

Monolithic Optofluidic Ring Resonator Lasers Created by Femtosecond Laser Nanofabrication

Hengky Chandrahalim[1], Qiushu Chen[1], Ali A. Said[2], Mark Dugan[2], and Xudong Fan[1*]

[1]Department of Biomedical Engineering, University of Michigan,
Ann Arbor, MI 48109, USA

[2]Translume Inc., 655 Phoenix Drive, Ann Arbor, MI, USA

*xsfan@umich.edu

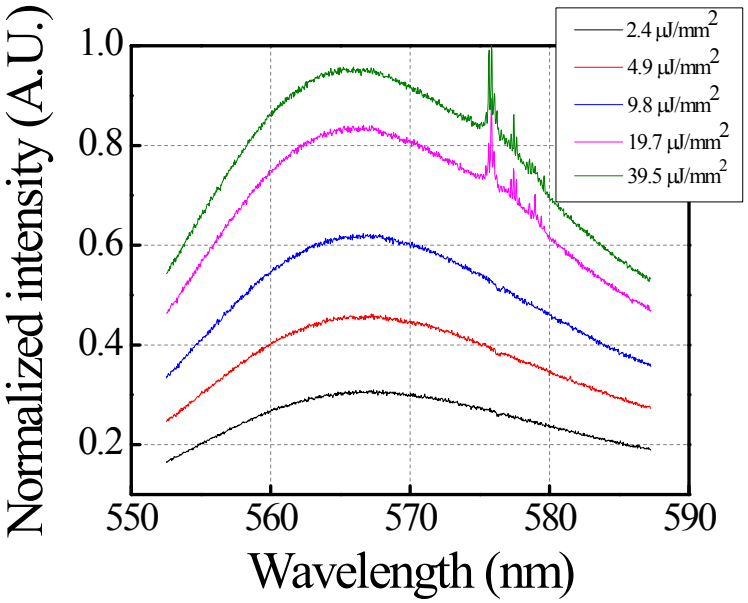

Supplementary Figure 1: Emission spectra as a function of pump fluence below and just above the lasing threshold. A 1200 g/mm grating was used to achieve wider spectral coverage. For comparison purposes, all emission spectra are normalized to the highest peak value. High resolution (0.05 nm) spectra using a 2400 g/mm grating are plotted in Fig. 4(A).

Table 1: Parameters used in the present work

Parameters	Definitions	Units
λ_P	Pump wavelength	nm
λ_L	Lasing wavelength	nm
λ_E	Fluorescence peak wavelength	nm
n_{Sol}	Refractive index of Solvent	-
n_T	Rhodamine 6G (R6G) dye concentration	cm^{-3}
n_X	Dye concentration at excited state	cm^{-3}
$\sigma_a(\lambda_P)$	Absorption cross-section at λ_P	cm^2
$\sigma_a(\lambda_L)$	Absorption cross-section at λ_L	cm^2
$\sigma_e(\lambda_L)$	Emission cross-section at λ_L	cm^2
$E(\lambda)$	Fluorescence quantum distribution	nm^{-1}
q	Quantum yield of RG6 in quinoline	-
q_{Ref}	Quantum yield of RHB in ethanol	-
$FL\text{-}Slope_{Sol}$	Fluorescence efficiency of RG6 in quinoline	nM^{-1}
$FL\text{-}Slope_{Ref}$	Fluorescence efficiency of RHB in ethanol	nM^{-1}
σ	Standard deviation of RG6 fluorescence distribution	ns
ε_{Sol}	Extinction coefficient of RG6	$M^{-1}cm^{-1}$
ε_{Ref}	Extinction coefficient of RHB	$M^{-1}cm^{-1}$
τ_F	Fluorescence lifetime	ns
A	$\sigma_A(\lambda_L)/\sigma_A(\lambda_P)$	-
B	$\sigma_A(\lambda_L)/\sigma_E(\lambda_L)$	-
C	$Q_{Dye}/\eta Q_0$	-
h	Planck constant	Js
c	Speed of light in vacuum	m/s
Δt	Pulse width of the pump laser	ns
η	Light coupling efficiency	-
P_{th}	Lasing photon density threshold	$\#photons/m^2$
Φ_{th}	Lasing fluence threshold	$\mu J/mm^2$
Q_{Dye}	Q-factor due to dye absorption	-
Q_{Sol}	Q-factor due to solvent absorption	-
Q_{Rad}	Q-factor due to radiation loss	-
Q_{Sc}	Q-factor due to scattering loss	-
Q_0	Q-factor of the laser cavity in the absence of gain medium	-

Q-factor analysis

Based on the lasing theory and the experimentally measured lasing threshold, the cavity Q-factor in the absence of the gain medium (*i.e.*, Q_0) can be calculated. The lasing threshold is given by:

$$n_X \sigma_E(\lambda_L) = (n_T - n_X)\sigma_a(\lambda_L) + \frac{2\pi n_{Sol}}{\lambda_L \eta Q_0} \tag{S1}$$

Equation (S1) can be written as:

$$\gamma \equiv \frac{n_X}{n_T} = \frac{\sigma_a(\lambda_L)}{\sigma_e(\lambda_L) + \sigma_a(\lambda_L)} \cdot (1 + \frac{Q_{Dye}}{\eta Q_0}) \tag{S2}$$

The stimulated emission cross section is obtained from the following expression:

$$\sigma_e(\lambda_L) = \frac{{\lambda_L}^4 E(\lambda_L)}{8\pi c {n_{Sol}}^2 \tau_F} \tag{S3}$$

According to the four energy level model, at steady state, γ relates to the dimensionless pump intensity by:

$$\gamma = \frac{I}{I+1}, \tag{S4}$$

and $$I = \frac{\gamma}{1-\gamma}, \tag{S5}$$

where $I = P \cdot \sigma_a(\lambda_p) \cdot \tau_F$. P is the power density in units of (# of photons per m^2 per second).

Equations (S2) and (S5) can be combined:

$$\frac{P_{th}}{\Delta t} \cdot \sigma_a(\lambda_P) \cdot \tau_F = \frac{\frac{\sigma_a(\lambda_L)}{\sigma_e(\lambda_L) + \sigma_a(\lambda_L)} \cdot [1+C]}{1 - \frac{\sigma_a(\lambda_L)}{\sigma_e(\lambda_L) + \sigma_a(\lambda_L)} \cdot [1+C]} = \frac{1}{\sigma_e(\lambda_L)} \frac{\sigma_a(\lambda_L) \cdot [1+C]}{1 - \frac{\sigma_a(\lambda_L)}{\sigma_e(\lambda_L)} \cdot C} \tag{S6}$$

P_{th} can be expressed in a simpler form as:

$$P_{th} = \frac{\Delta t}{\sigma_e(\lambda_L) \cdot \tau_F} A \frac{1+C}{1 - B \cdot C} \tag{S7}$$

where $A = \frac{\sigma_a(\lambda_L)}{\sigma_a(\lambda_P)}$, $B = \frac{\sigma_a(\lambda_L)}{\sigma_e(\lambda_L)}$, and $C = \frac{Q_{Dye}}{\eta Q_0}$.

Q_{Dye} can be calculated by:

$$Q_{Dye} = \frac{2\pi n_{Sol}}{\lambda_L n_T \sigma_a(\lambda_L)} \tag{S8}$$

P_{th} is related to the excitation fluence at the pump wavelength by:

$$\Phi_{th} = P_{th} \cdot \frac{h \cdot c}{\lambda_P} = \frac{h \cdot c \cdot \Delta t}{\sigma_e(\lambda_L) \cdot \lambda_P \cdot \tau_F} A \frac{1+C}{1 - B \cdot C} \tag{S9}$$

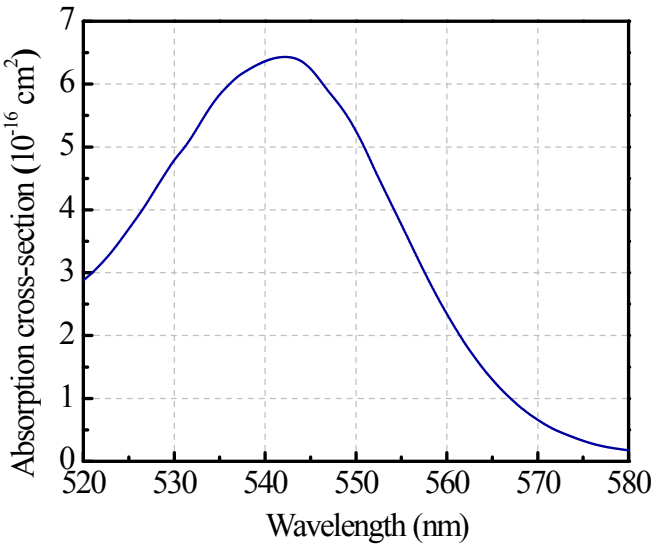

Supplementary Figure 2: Absorption cross-section of RG6 in quinoline based on absorbance measurement with 10 μM solution.

In order acquire necessary parameters to analyze Q_0 in equation (S9), we performed several measurements and data extractions. We measured the Rhodamine 6G (R6G) dye absorption cross-section as presented in Fig. S2 and obtained $\sigma_a(\lambda_P)$ and $\sigma_a(\lambda_L)$. Q_{Dye} was calculated to be 9.07×10^3 according to equation (S8).

Next, we need to determine the fluorescence quantum distribution $E(\lambda)$ and fluorescence lifetime (τ_F) of the RG6 in quinoline to calculate $\sigma_e(\lambda_L)$ in equation (S3). In order to compute $E(\lambda)$, we need to first calculate the quantum yield (q) and measure the fluorescence spectrum of the dye solution. To determine the quantum yield, we performed absorption and fluorescence measurements of RG6 dye in quinoline and compared the results against a reference dye solution (Rhodamine B (RhB) in ethanol) which has a known q_{Ref} value[1]. Fluorescence test was done with FluoroMax-4

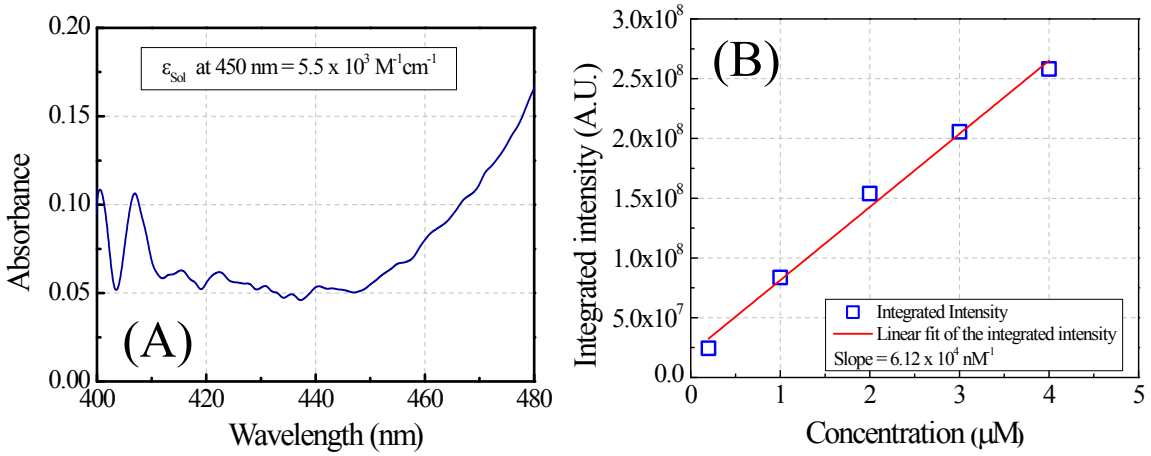

Supplementary Figure 3: (A) Absorbance of RG6 dye in quinoline as a function of wavelength. (B) Integrated fluorescence intensity as a function of RG6 dye concentration.

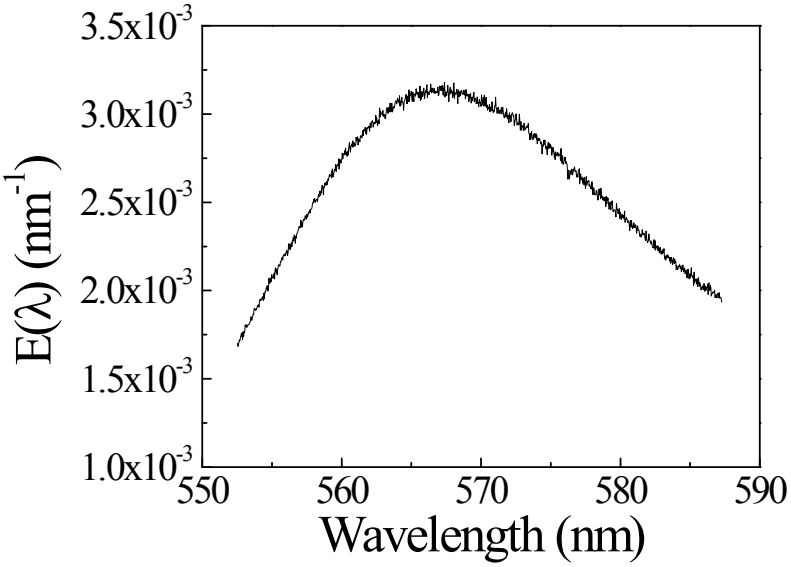

Supplementary Figure 4: Fluorescence quantum distribution, E(λ).

spectrofluorometer (Horiba Scientific). Absorption test was performed with NanoDrop 2000c spectrophotometer (Thermal Scientific). The excitation wavelength for the absorption measurement was 450 nm. The measurement results shown in Fig. S3 indicate ε_{Sol} and FL-Slope$_{Sol}$ of 5.5 x 10^3 $M^{-1}cm^{-1}$ and 6.12 x 10^4 nM^{-1}, respectively.

Using the equation:

$$q = q_{Ref} \times \frac{FL - Slope_{Sol}}{FL - Slope_{Ref}} \times \frac{n_{Sol}^2}{n_{Ref}^2} \times \frac{\varepsilon_{Ref}}{\varepsilon_{Sol}} \quad \text{(S10)}$$

the fluorescence quantum yield, q, of 0.12 was obtained.

RG6 fluorescence quantum distribution, E(λ), can be obtained through the fluorescence spectrum in Fig. S1(B) by considering that

$$\int E(\lambda) \cdot d\lambda = q. \quad \text{(S11)}$$

According to Fig. S4

$$E(575\ nm) = 0.0028\ nm^{-1}. \quad \text{(S12)}$$

In the next step, we measured the fluorescence lifetime, τ_F of the RG6 in quinoline. The measurement result of the time correlated photon counting experiment performed using a fluorescence lifetime spectrometer (TemPro, Horiba) is shown in Fig. S4. An exponential fit reveals 5.88 ns fluorescence lifetime of RG6 dye in quinoline. We substituted the measured parameters to equation (S3), and determined the stimulated emission cross-section, σ_e, of 2.61x10^{-17} cm^2.

We have now all the parameters needed to extract Q_0 from equation (S9). Considering an input pump fluence threshold (Φ_{TH}) of 15 μJ/mm^2 during experiment, we calculate Q_0 to be 3.3x10^4.

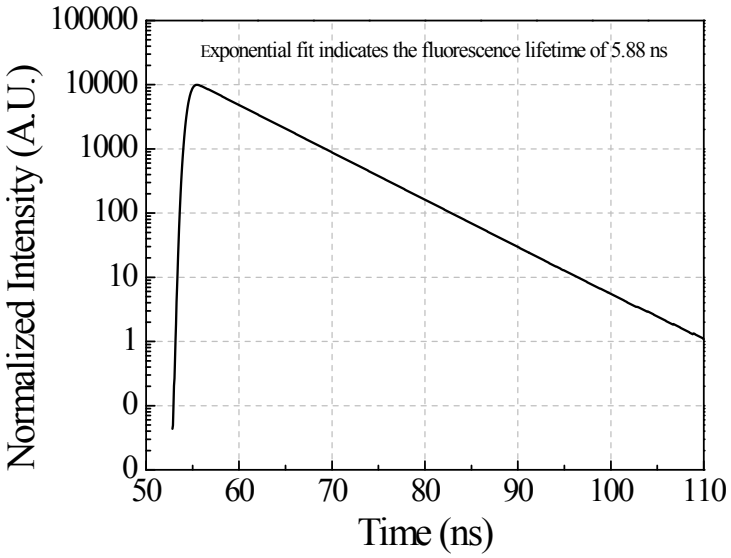

Supplementary Figure 5: Fluorescence decay curve obtained with 500 μM RG6 dye in quinoline. The exponential fit reveals 5.88 ns fluorescence lifetime.

In order to validate the method used here to extract the Q-factor (*i.e.*, Q_0), we employ the same theoretical model to estimate the lasing threshold of an optofluidic ring resonator laser reported in Ref. 2., which Q-factor is known (*i.e.*, $\eta Q_0 = 4x10^6$). Table 2 tabulates several key parameters used for this work and the work reported in reference[2]. Based on the parameters listed on the right column of Table 2, an estimated lasing fluence threshold of 22 nJ/mm^2 is obtained, very close to the experimentally measured result of 25 nJ/mm^2. Therefore, our current approach to extract $Q_0 = 3.3x10^4$ using the lasing fluence threshold is justified.

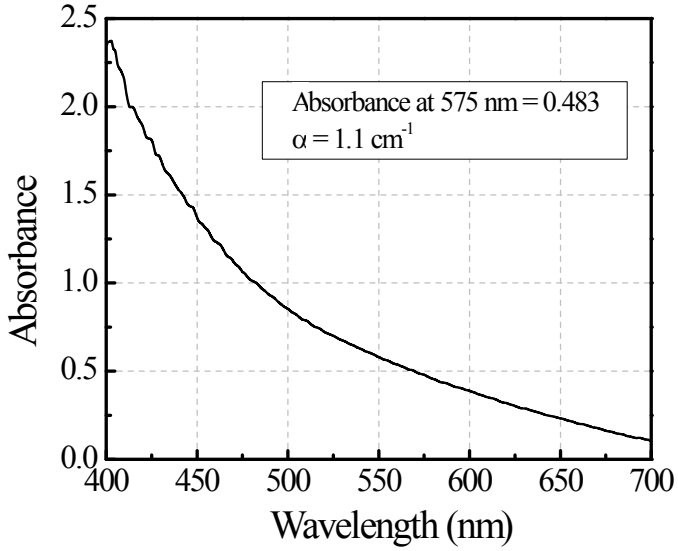

Supplementary Figure 6: Absorbance measurement of quinoline as a function of wavelength.

Table 2: Comparisons of the current work and the work in Ref. 2.

Parameters	Current work (1 mM R6G in quinoline)	Ref. 2 (2 mM R6G in ethanol)
λ_P	532 nm	532 nm
λ_L	575 nm	600 nm
n	1.62	1.40
n_T	6×10^{17} cm^{-3}	1.2×10^{18} cm^{-3}
$\sigma_a(\lambda_P)$	5.18×10^{-16} cm^2	2×10^{-16} cm^2
$\sigma_a(\lambda_L)$	3.25×10^{-17} cm^2	1×10^{-19} cm^2
$\sigma_e(\lambda_L)$	2.61×10^{-17} cm^2	1×10^{-16} cm^2
$E(\lambda)$	2.8×10^{-3} nm^{-1}	5.7×10^{-3} nm^{-1}
q	0.12	0.9
τ_F	5.88 ns	4.08 ns
A	6.27×10^{-2}	5×10^{-2}
B	1.25	1×10^{-3}
C	0.28	0.3
Δt	5 ns	5 ns
Q_{Dye}	9.07×10^3	1.2×10^6
ηQ_0	3.3×10^4	4×10^6
Φ_{th}	15 μJ/mm^2	22 nJ/mm^2

Estimation of Q_{Sc}

The surface roughness of a pre-annealing device fabricated by the 3-D femtosecond laser writing process has previously been characterized to be 40-50 nm[3]. Fig. S6 shows the SEM image of the ring resonator inner wall taken after the ring resonator underwent thermal annealing. The roughness was reduced to approximately 30 nm.

The roughness is related the Q-factor by[4]:

$$Q \propto \frac{1}{\sigma_{rough}^{\ 2} \cdot (n_{core}^{\ 2} - n_{cladding}^{\ 2})}, \tag{S13}$$

where σ_{rough} is the surface roughness. n_{core} and $n_{cladding}$ are the refractive index for the ring and the cladding, respectively. Previous work on polymer ring resonators, whose surface roughness and the Q-factor have been well characterized and directly measured, provides a means to estimate the scattering loss related Q-factor of our ring resonator. According to Ref. 4,5, a Q-factor of $5x10^5$ was obtained at 780 nm for a polymer ring resonator with the surface roughness of 5-10 nm. Based on equation S13, the scattering loss related Q-factor of our ring resonator should range between $3.2x10^4$ and $1.3x10^5$, in agreement with the scattering related Q-factor estimation ($Q_{Sc} = 4.2x10^4$) that we extract based on the lasing threshold.

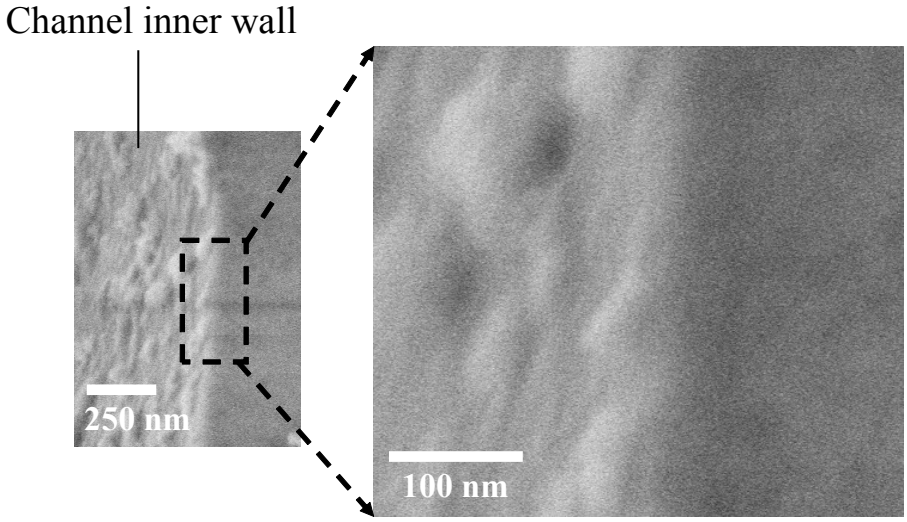

Supplementary Figure 7: SEM images of the channel inner wall. The surface roughness (rms) is about 30 nm.

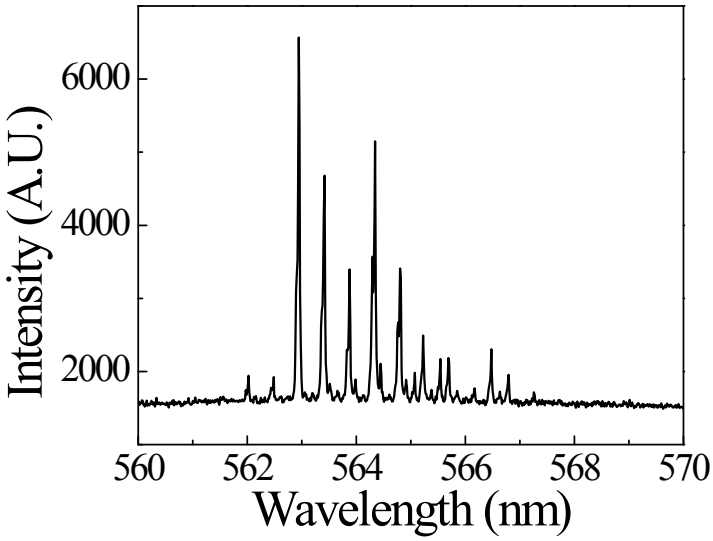

Supplementary Figure 8: Lasing emission from 1 mM R6G in chlorobenzene (n=1.524) at a pump fluence of 90 μJ/mm^2. Flow rate was 3 μL/min.

References

1. F. L. Arbeloa, P. R. Ojeda, and I. L. Arbeloa, "Fluorescence self-quenching of the molecular forms of Rhodamine B in aqueous and ethanolic solutions," J. Lumin. **44**, 105-112 (1989).
2. S. Lacey, I. M. White, Y. Sun, S. I. Shopova, J. M. Cupps, P. Zhang, and X. Fan, "Versatile opto-fluidic ring resonator lasers with ultra-low threshold," Opt. Express **15**, 15523-15530 (2007).
3. Y. Sikorski, C. Rablau, M. Dugan, A. A. Said, P. Bado, and L. G. Beholz, "Fabrication and characterization of microstructures with optical quality surfaces in fused silica glass using femtosecond laser pulses and chemical etching," Appl. Opt. **28**, 7519-7523 (2006).
4. C.-Y. Chao, and L. J. Guo, "Reduction of Surface Scattering Loss in Polymer Microrings Using Thermal-Reflow Technique," IEEE Photon. Technol. Lett. **16**, 1498-1500 (2004).
5. T. Ling, S.-L. Chen, and L. J. Guo, "High-sensitivity and wide-directivity ultrasound detection using high Q polymer microring resonators," Appl. Phys. Lett. **98**, 204103 (2011).